Chapter 14
Photoenergy Conversion

Yohei Ishida and Shinsuke Takagi

14.1 Introduction

Inorganic nanosheets are utilized for converting or harvesting energy. The modern world is reliant on the use of energy in various forms, including photo, electrical, chemical, potential, mechanical, nuclear, and thermal energy. Efficient interconversion among these energy forms is crucial to the functioning of today's society. This chapter will focus on the conversion of photoenergy into other forms of energy using inorganic nanosheets. Inorganic nanosheet-based photoenergy conversion materials have an advantage due to their unique properties, such as highly crystalline two-dimensional surfaces, high aspect ratios, and the separation of the front and back sides by atomically thin surfaces. Inorganic nanosheet-based photoenergy conversion has been reported in various fields, and this chapter briefly reviews the conversion of photoenergy into chemical, electrical, and mechanical energy, as well as other photoenergies (wavelength conversion or light harvesting).

Y. Ishida
Division of Material Science and Engineering, Faculty of Engineering,
Hokkaido University, Kita 13, Nishi 8, Kita-Ku, Sapporo, Hokkaido 060-8628, Japan

S. Takagi (✉)
Department of Applied Chemistry, Graduate Course of Urban Environmental Sciences,
Tokyo Metropolitan University, Minami-Ohsawa 1-1, Tokyo 192-0397, Japan
e-mail: takagi-shinsuke@tmu.ac.jp

T. Nakato et al. (eds.), *Inorganic Nanosheets and Nanosheet-Based Materials*,
Nanostructure Science and Technology, DOI 10.1007/978-4-431-56496-6_14

14.2 Conversion of Photoenergy into Chemical Energy

Photocatalysis, the general process of converting photoenergy into chemical energy, has been extensively investigated since Fujishima and Honda first reported photocatalytic water splitting using a titanium dioxide (TiO_2) semiconductor [1]. TiO_2 photocatalysis has been developed for use in both organic pollutant degradation and hydrogen generation via water splitting.

Among various oxide semiconductor photocatalysts [2], TiO_2 has proven the most suitable for widespread use in solar energy conversion and environmental applications due to its chemical inertness, strong oxidizing power, low cost, and long-term stability. Moreover, exfoliated titanium oxide nanosheets have received considerable attention [3].

As exfoliated nanosheets in suspension provide almost infinite available spaces for guest species to homogeneously adsorb the nanosheet surfaces, nanosheet-based photocatalysts are expected to have unique characteristics.

The photocatalytic decomposition of harmful organic compounds in water or air is a promising process for environmental remediation and has been studied using titania nanosheet photocatalysts under UV irradiation. For example, the nanocomposite prepared by pillaring $Ti_{0.91}O_2^{0.36-}$ nanosheets with TiO_2 nanoparticles via an exfoliation-reassembly process efficiently decomposed organic pollutants such as methylene blue and 4-chlorophenol under UV light irradiation [4].

Photocatalytic water splitting for hydrogen generation using titania nanosheets has also been reported. As the conduction band minimum position of layered titanate is only slightly higher than the redox couple potential of H^+/H_2, titania nanosheets do not provide strong reduction for water splitting. For example, nitrogen-doped titanate exhibited apparent visible-light absorption up to 450 nm [5], whereas its performance in water splitting for hydrogen generation was nearly negligible. Osterloh and co-workers systematically studied the change in the optical, vibrational, electronic, and photocatalytic properties of multi-layered titanates $A_2Ti_4O_9$ (A = K, H, TBA) [6]. The catalytic activity of all titanates was limited by the potential of the conduction band edge, which is too low for efficient H_2 evolution in a neutral solution (Fig. 14.1). With the assistance of cocatalysts, such as Pt metal, $Ti_{0.91}O_2^{0.36-}$ exhibited a moderate hydrogen production yield. Loading with Pt shifted the band edge of all titanates toward oxidizing potentials (Fig. 14.1), which was attributed to Fermi level equilibration across the titanate-platinum interface.

Layered niobate is one of the other examples of a nanosheet-based photocatalyst, although Nb_2O_5 is not a photocatalyst under UV irradiation [7]. Chemical exfoliation of $K_4Nb_6O_{17}$ and the similarly structured Dion–Jacobsen phase $KCa_2Nb_3O_{10}$ produces 1 nm thin single-crystalline nanosheets or scrolls. The crystalline nanosheets and their Pt and IrO_2-modified derivatives showed photocatalytic activity in water splitting [7–9].

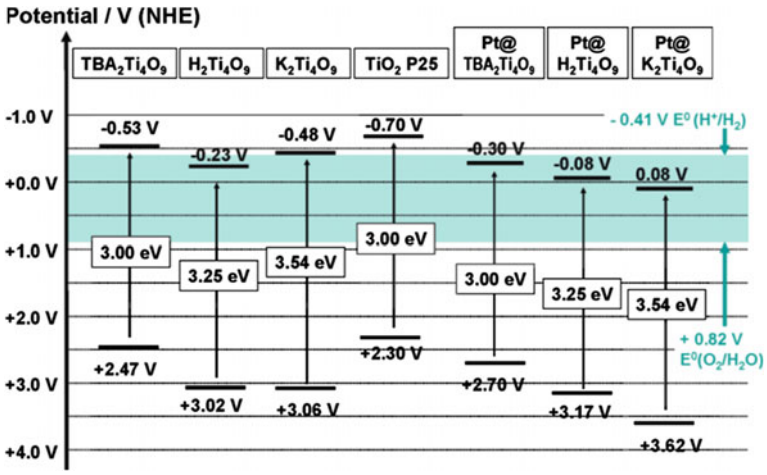

Fig. 14.1 Band gap potentials of various layered titanate and $Ti_4O_9^{2-}$ nanosheets determined by optical and photoelectrochemical measurements. Experimental data for TiO_2 P25 nanoparticles are included for comparison. Reprinted with permission from Ref. [6] (copyright 2010, American Chemical Society)

14.3 Conversion of Photoenergy into Electrical Energy

Devices used to convert photoenergy into electrical energy are generally called photovoltaic devices. Several types of efficient and mature photovoltaic devices have been developed, and can be distinguished according to their content and structure. Well-established photovoltaic materials on inorganic bases include silicon, III-V and II-VI PN junctions, and copper-indium-gallium-selenium (CIGS) photovoltaic devices [2].

As described in the previous chapter, TiO_2 is the most common semiconductor photocatalyst, but it is also widely used in photovoltaic devices [2, 3]. The rapid transport and transfer of photogenerated electrons in these TiO_2 films is pivotal to improving the conversion efficiency from photoenergy to electrical energy. Generally, TiO_2 nanoparticles with a diameter of 10–20 nm were used; hence, the obtained film was usually transparent with little light scattering. The incorporation of relatively large particles (above 100 nm) has been employed at light-scattering centers to increase the optical length of the film, and enhanced light harvesting has been demonstrated [10]. The use of two-dimensional nanosheets with sizes approaching 100 nm should have a similar effect. As a result, such materials are expected to exhibit high light-harvesting efficiency and fast charge carrier motion due to the 2D crystalline surfaces.

To this end, Haga and co-workers reported novel photoelectrochemical devices using titania nanosheets with Zn porphyrin molecules fabricated by layer-by-layer techniques (Fig. 14.2) [11]. Closely packed titania nanosheet ($Ti_{0.91}O_2$) monolayers on indium tin oxide (ITO), mica, and quartz surfaces strongly adsorbed cationic

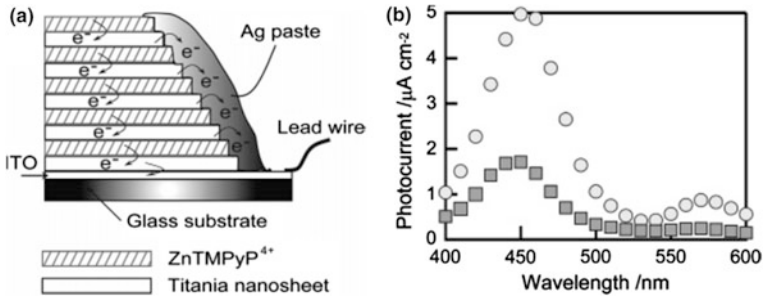

Fig. 14.2 **a** Schematic illustration of graduated multilayer film with Ag paste on an ITO electrode, **b** photocurrent action spectra of [($ZnTMPyP^{4+}$/titania nanosheet)$_5$/ITO] + Ag paste (*circle*) and ($ZnTMPyP^{4+}$/titania nanosheet)$_5$/ITO (*square*). Reprinted with a slight modification with permission from ref [11] (copyright 2007, American Chemical Society)

[5,10,15,20-tetrakis(1-methylpyridinium-4-yl)porphyrinatozinc]$^{4+}$ ($ZnTMPyP^{4+}$) via electrostatic interactions.

The visible-light irradiation of this multilayer film on an ITO electrode in the presence of triethanolamine as an electron donor resulted in an anodic photocurrent. The quantum yield for photocurrent generation by this two-layer film, with the electrode structure ITO/titania nanosheet/$ZnTMPyP^{4+}$, was estimated to be 8.63%. The titania nanosheet itself has a wide band gap (3.8 eV) due to the 2D quantum size effect. This caused vertical electron transport efficiency, through the alternately layered titania nanosheets and organic dyes such as $ZnTMPyP^{4+}$ on the solid surface, to lower as the number of layers increased due to the succession of vertical energy barriers. To overcome this limitation, the use of a lateral interlayer connection of all titania nanosheets with Ag paste was also examined, resulting in a significant improvement in photocurrent density compared with the bare titania nanosheet-$ZnTMPyP^{4+}$ system. Other types of inorganic nanosheets, such as $Ca_2Nb_3O_{10}^-$, $TiNbO_5^-$, $Ti_2NbO_7^-$, and $Ti_5NbO_{14}^{3-}$, have also been reported as novel photovoltaic materials [12].

14.4 Conversion of Photoenergy into Mechanical Energy

Photoresponsive mechanical materials are usually defined as having macroscopic-scale morphologies that are reversibly changed by photoirradiation. These materials are promising for applications in light-driven actuators and artificial muscles that are able to convert the photoenergy into mechanical energy. Many excellent photoresponsive mechanical materials have been reported, such as molecular single crystals [13], and liquid crystal polymers [14].

For this purpose, Inoue and co-workers focused on the use of inorganic nanosheets [15, 16]. They reported that upon photoirradiation of layered $K_4Nb_6O_{17}$

intercalated with a polyfluoroalkyl azobenzene surfactant, a very large magnitude lateral movement (sliding) of the nanosheets was reversibly induced. Nanosheet sliding has been clearly observed in a cross section of layered hybrid film, as a result of concomitant reversible *cis-trans* isomerization of the azobenzene moiety. Using photoirradiation at 368 and 463 nm, the total reversible sliding motion of the layered hybrid film reached ~1500 nm in the lateral direction. Furthermore, the thickness of the hybrid film (~450 nm) was reversibly changed by up to ±18 nm as each interlayer space shrank and expanded due to photoisomerization of the intercalated azobenzene derivative. This work shows that nanosheet-based photoinduced mechanical materials have an advantage due to their large two-dimensional surfaces and high aspect ratios.

14.5 Wavelength Conversion of Photoenergy and Light Harvesting

14.5.1 Theory of Förster Resonance Energy Transfer

Förster (or fluorescence) resonance energy transfer (FRET) is the transfer of photoexcitation energy from a donor fluorophore to an acceptor [17–19].

$$A^* + B \rightarrow A + B^* \tag{14.1}$$

Here, * denotes the electrically excited state, A and B denote energy donor and energy acceptor molecules, respectively.

The reaction rate constant for FRET is expressed as shown in Eq. 14.2,

$$k_{ET} = \frac{9\phi_D \kappa^2 ln10}{128\pi^5 n^4 N_A \tau_D R^6} \int f_D(v)\varepsilon_A(v)\frac{dv}{v^4} \tag{14.2}$$

where ϕ_D is the fluorescence quantum yield of the donor, n is the refractive index of the medium, N_A is Avogadro's number, κ^2 is the dipole orientation factor, τ_D is the excited lifetime of the donor in the absence of an acceptor, R is the distance between the donor and the acceptor, and the integral part represents the spectral overlap between the absorption spectrum of the energy acceptor and fluorescence spectrum of the energy donor. As can be seen from Eq. 14.2, the energy-transfer rate constant is inversely proportional to the sixth power of R. A large spectral overlap integral between the absorption spectrum of the energy acceptor and the fluorescence spectrum of the energy donor is necessary for efficient energy transfer. Moreover, a parallel arrangement of the transition dipoles enhances the FRET efficiency and a perpendicular orientation prevents FRET (expressed as κ^2 in Eq. 14.2) [20]. Generally, FRET phenomena are observable at donor–acceptor distances of around 20–60 Å when the spectral overlap is large enough [21–27].

Since FRET is a highly sensitive spectroscopic measurement technique for processes occurring on the nanometer and sub-nanometer scale, it has been widely used for qualitative and quantitative biochemical applications, such as DNA sequencing [28]. Moreover, a light-harvesting antenna in natural photosynthetic bacteria realizes highly efficient photoexcited energy-transfer processes for photosynthesis [29]. This has strongly encouraged researchers to study synthetic molecular or supramolecular FRET systems for artificial photosynthesis and artificial light-harvesting systems.

While research on FRET has been mainly focused on synthetic molecular systems, supramolecular biosystems (with DNA, peptides, etc.), or quantum dots, nanosheets have been well used in the twenty-first century [30]. The methodologies of using nanosheets can be categorized into two series: (1) the use of nonphotofunctional nanosheets as FRET reaction fields for organic guests, and (2) the use of photofunctional nanosheets as a FRET donor or acceptor. The advantages of such FRET research on 2D nanosheets are (i) effective control of κ^2 according to the 2D reaction field [20], (ii) ease of handling the materials due to their large size (several tens to thousands of nm), (iii) additionally, the photophysical characteristics of organic guests such as fluorescence quantum yields or lifetimes are sometimes enhanced [31, 32] by adsorption onto atomically flat 2D surfaces. Recent results on 2-dimensional FRET utilizing nanosheets will be reviewed.

14.5.2 *Nonphotofunctional Nanosheets as FRET Reaction Fields for Organic Guests*

Typical, anionic charged-clay minerals are useful materials for nonphotofunctional nanosheets because of their chemical stability, optical transparency in the visible region, and ease of handling [33]. Cationic guest molecules can form stable complexes through electrostatic interactions (and through hydrophobic interactions when applied in aqueous solution).

From the various types of anionic clay minerals, saponite (of the smectite group) is the focus of this chapter due to its suitable charge density. The typical chemical formula of saponite clay is expressed as $[(Si_{7.20}Al_{0.80})\text{-}(Mg_{5.97}Al_{0.03})O_{20}(OH)_4]^{-0.77}(Na_{0.77})^{+0.77}$. The experiments presented here have been carried out using an aqueous suspension of exfoliated single saponite nanosheets at low concentrations.

It is well known that organic molecules tend to aggregate and/or segregate on inorganic surfaces, mainly because of hydrophobic interactions and Van der Waals interactions between the organic molecules [34, 35]. Since H-aggregation and irregular aggregation drastically decrease the excited-state lifetime, efficient photochemical reactions such as FRET had been considered difficult in clay/dye complexes.

Uniform molecular adsorption on saponite surfaces was realized in the pioneering work by Takagi and Inoue in 2002 (Fig. 14.3) [36, 37]. Systematic experiments using numerous cationic porphyrin derivatives showed that a porphyrin molecule, which has a specific molecular structure, can be adsorbed on clay surfaces without concomitant aggregation, even under high-density conditions. Such nonaggregated alignment results from distance matching due to guest—host Coulombic interactions between the positively charged dye molecules and the negatively charged-clay surface. This effect was termed the "size-matching effect." The average center-to-center intermolecular distance was determined to be 2.4 nm under saturated adsorption conditions based on a hexagonal array. This value is most interesting from the viewpoint of photochemistry, because the interaction between the transition moments of adjacent porphyrin molecules (aggregation) is negligible; however, interactions in the excited state are possible. Thus, efficient photochemical reactions such as FRET are expected.

FRET between two different kinds of porphyrins (*m*-TMPyP(D) and *p*-TMPyP (A)) was investigated by steady-state and time-resolved fluorescence measurements [38]. A decrease in donor fluorescence and an increase in acceptor fluorescence were observed as the dye loading increased (Fig. 14.4 left). Clear isoemissive points were observed, as indicated by the arrows in the figure.

In Fig. 14.4 right, the energy-transfer efficiencies (η_{ET}) are plotted against the porphyrin loading levels. η_{ET} increased with increasing porphyrin loading levels, because the average intermolecular distance between the porphyrins decreased. Notably, the maximum η_{ET} reached $\sim$100% at higher acceptor ratios and dye loadings. The mechanism of the FRET process has been investigated by time-resolved fluorescence spectroscopy.

In spite of the advantages of saponite–porphyrin systems, a limitation is that anionic clay nanosheets could only be used as hosts for cationic adsorbent molecules. Neutral molecules, such as aromatics, do not adsorb on these surfaces. A new strategy has been developed to overcome this problem. The strategy involved a supramolecular approach in which a cationic organic host system, which included a neutral guest molecule, was adsorbed on anionic saponite surfaces [39, 40].

A cavitand containing eight ammonium groups (octaamine, OAm [41]) was used as the host for neutral organic molecules (Fig. 14.5). Strong Coulombic attractions

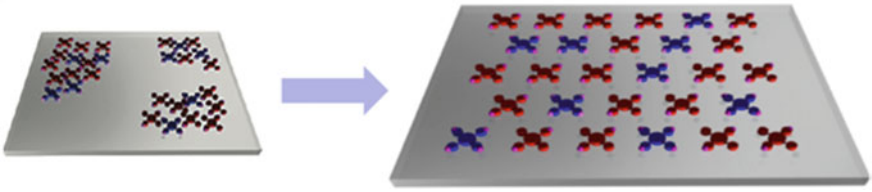

Fig. 14.3 Schematic representation of a saponite/porphyrin supramolecular complex. The guest porphyrins adsorb on the saponite surface as monomers without aggregation through the "size-matching effect." Reprinted with permission from Ref [38] with a slight modification (copyright 2011, American Chemical Society)

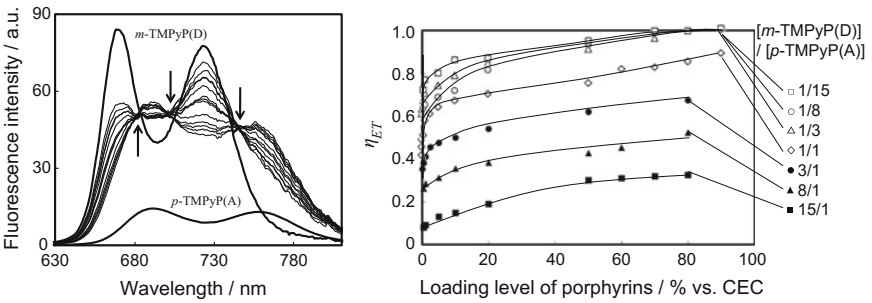

Fig. 14.4 *Left.* The fluorescence spectra for *m*-TMPyP(D)/*p*-TMPyP(A)/saponite complexes. The *thick lines* are the individual fluorescence spectra of the *m*-TMPyP(D)/saponite and *p*-TMPyP(A)/saponite complexes. The *arrows* indicate isoemissive points. *Right.* The energy-transfer efficiencies at various loading levels and ratios of porphyrins. Reprinted with permission from Ref. [38] (copyright 2011, American Chemical Society)

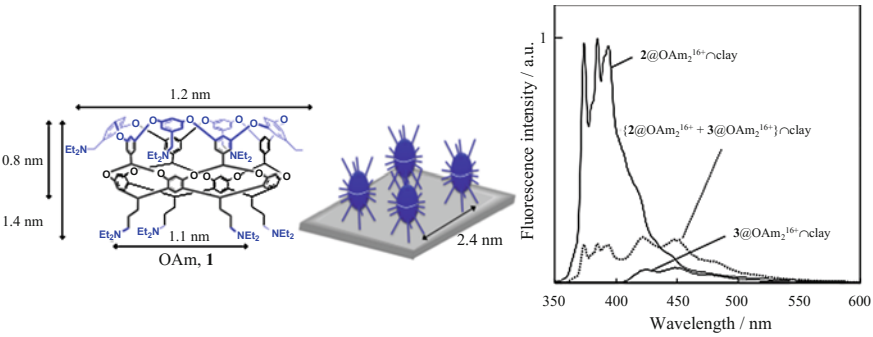

Fig. 14.5 Structure of octaamine cavitand (OAm, **1**), a plausible adsorption structure model of guest@OAm_2^{16+} on saponite surfaces under maximum adsorption conditions, and fluorescence spectra for the {**2**@OAm_2^{16+} + **3**@OAm_2^{16+}} ∩ clay complex and respective **2**@OAm_2^{16+} ∩ clay and **3**@OAm_2^{16+} ∩ clay complexes. Reprinted with permission from Ref. [40] with a slight modification (copyright 2013, American Chemical Society)

between the ammonium groups and the anionic saponite anchored OAm to the nanosheets. Since OAm forms capsular assemblies with neutral organic guest molecules, energy transfer between two OAm capsules, one containing a donor molecule (pyrene, **2**) and the other encapsulating an acceptor molecule (2-acetylanthracene, **3**), adsorbed on saponite surfaces was investigated [40]. The efficient FRET between **2**@OAm_2^{16+} (pyrene encapsulated within two OAm^{8+} species) and **3**@OAm_2^{16+} adsorbed on saponite nanosheets was demonstrated by monitoring the fluorescence intensities and lifetimes. With increased loading levels of guests, the fluorescence intensity of donor **2** decreased, while that of acceptor **3** increased (Fig. 14.5 right). This suggested the possibility of FRET in the current system. η_{ET} was determined to be 85%. As expected, owing to the decreased intermolecular distance, η_{ET} increased with the loading level. By the detailed

time-resolved fluorescence measurement, FRET rate constant was calculated to be $1.4 \times 10^7\ s^{-1}$.

As summarized above, supramolecular surface photochemistry has undergone significant development recently [37, 38, 42–44]. Recent developments and understandings of molecular attitudes on inorganic surfaces greatly encourage the application of these nanosheet–dye systems in photonics fields.

14.5.3 Photofunctional Nanosheets as FRET Donor/Acceptors

Some photofunctional nanosheets, such as graphene oxide or transition metal dichalcogenides, have been used as FRET donor or acceptors in combination with other organic dyes or quantum dots. In this chapter, FRET phenomena utilizing the excited state of nanosheet materials will be reviewed.

Graphene is a one-atom-thick planar sheet of sp^2-bonded carbon atoms ordered in a two-dimensional honeycomb lattice [45]. Graphene oxide (GO) consists of a similar atomically thin structural lattice, but possesses oxygen-containing functional groups [46]. Consequently, GO possesses recombined electron–hole pairs localized within a small sp^2 carbon domain embedded in a sp^3 matrix, and displays photoluminescence properties. Due to its heterogeneous structure containing various densities and distributions of carboxyl or hydroxyl groups, predominantly arising from differences in synthesis processes, GO can be fluorescent over a broad range of wavelengths from the near IR to UV regions. Thus, GO can be used as a FRET donor or acceptor when its emission wavelength is properly controlled [47–49].

Dong and co-workers demonstrated the first efficient FRET between quantum dots (QDs) and GO for biosensing applications [50]. Specifically, CdTe QDs, conjugated with a molecular beacon (MB), were used to detect DNA concentration and sequence, as well as to detect proteins such as thrombin. By the surface modification of QDs with a MB, the FRET between QDs and GO and the strong interaction between the ssDNA of the MB loop structure and GO were combined to develop a novel sensitive and selective platform for fluorescence quenching detection of DNA. Upon recognition of the MB to the target, the increasing QD-GO distance and the weakened DNA-GO interaction significantly hindered the FRET, and thus, increased the fluorescence of the QDs (Fig. 14.6 left).

The specificity of the MB-QD probe was studied using three kinds of DNA sequences, including a perfectly complementary target, a single-base mismatched strand, and a three-base mismatched strand. Specifically, the MB-QD probe differentiated between the perfectly complementary target, single-base mismatched strand (signal was 40% of that of the perfectly complementary target), and three-base mismatched strand (signal was 15%). Moreover, the quenching efficiency was much higher for MB-QDs than the typical efficiency seen in MB-based detection, which helped to improve the achievable sensitivity and dynamic range.

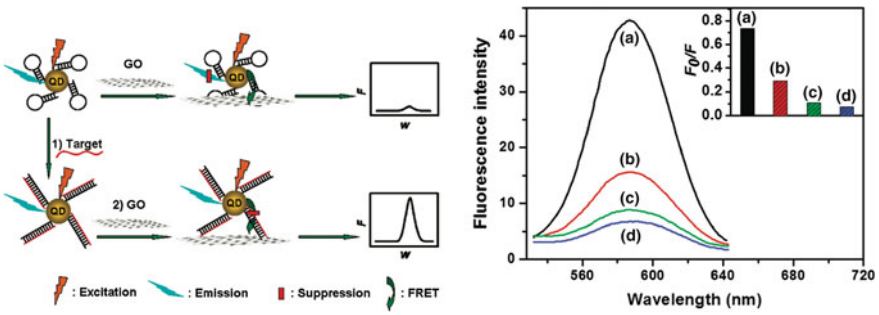

Fig. 14.6 Left: Schematic representation of GO-induced fluorescence quenching of MB-QDs and the biosensing mechanism through FRET. *Right* Fluorescence spectra of MB-QDs after incubation with **a** target, **b** single-base mismatch stand, **c** three-base mismatch stand, and **d** no target, followed by addition of GO for 5 min. Inset: fluorescence intensity ratio F_0/F. Reprinted with permission from ref [50] (copyright 2010, American Chemical Society)

These results demonstrated that the proposed approach could effectively detect the target with high specificity and had potential applications in single nucleotide polymorphism analysis.

Single- or several-layered transition metal dichalcogenides (TMDs) are another example of photofunctional–nanosheet-based FRET [51, 52]. TMDs are generally expressed as MX_2, where M is a transition metal of groups 4–10 and X is a chalcogen. Exfoliation of the bulk TMDs into mono- or few-layer structures largely preserves their properties, and also leads to additional characteristics due to confinement effects.

Molybdenum disulfide (MoS_2) is a widely known layered TMD. It is an indirect-band-gap semiconductor with an energy gap of $\sim$1.29 eV in the bulk form (although it does not show virtual emission) and has also attracted interest as a photovoltaic and photocatalytic material. The band gap of MoS_2 increases on decreasing crystal thickness below 100 nm due to quantum confinement effects, and the quantum yield drastically increases from the bulk form. In addition to the increase in its size, the nature of the band gap also changes from indirect to direct when the thickness reaches a single monolayer. Recent success in isolating MoS_2 monolayers has allowed the observation of strong photoluminescence that can be attributed to the direct-gap electronic structure of monolayer MoS_2 [53].

Prins and co-workers have recently reported systematic FRET phenomena from colloidal quantum dots to exfoliated monolayer and few-layer MoS_2 [54]. They used CdSe/CdZnS core/shell QDs, whose emission spectrum overlaps with the direct excitonic absorption of MoS_2. Monolayer and few-layer MoS_2 nanosheets were deposited on Si/SiO_2 substrates, and QDs were deposited by spin-coating to form a submonolayer that is uniformly $\leq$1-QD thick.

Figure 14.7a shows a bright-field optical micrograph of a MoS_2 flake prior to the deposition of QDs. The different colors indicate that there are several thicknesses present. For the observed region in Fig. 14.7a, the thickness was identified by micro-Raman measurements as bulk-like thickness (>8 layers) down to monolayer

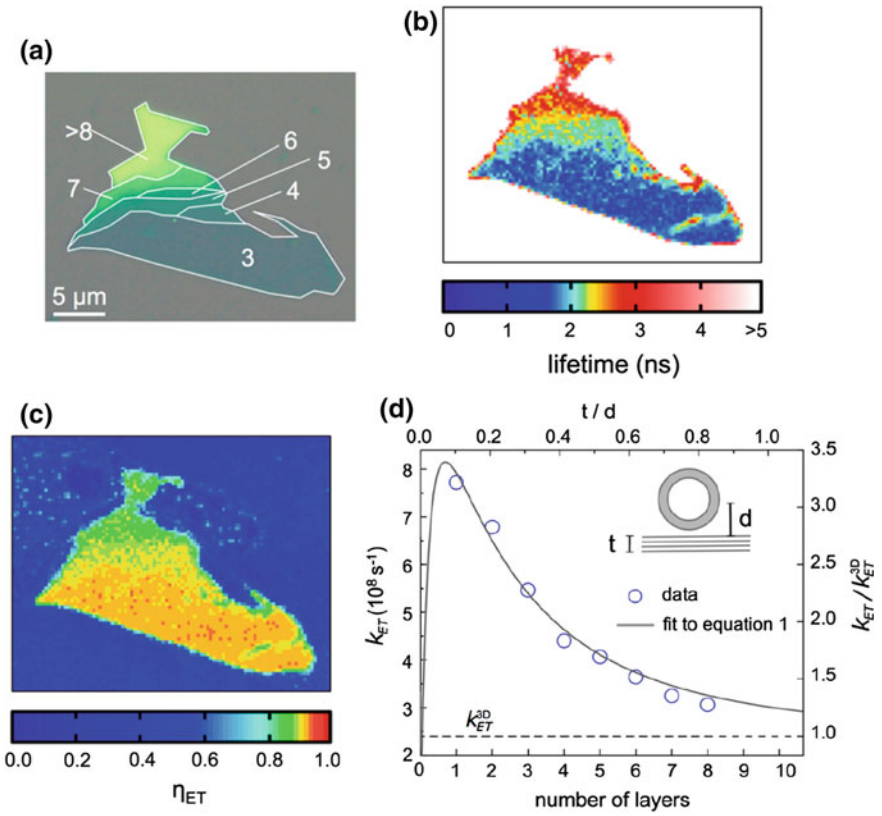

Fig. 14.7 **a** Optical micrograph of a mechanically exfoliated MoS_2 flake with indicated layer thicknesses of the different facets. **b** QD fluorescence lifetime map of the same flake with a saturated color scale to emphasize the lifetime variations within the flake area. **c** Energy-transfer efficiency map of the same flake. Scale bar is identical for all three panels. **d** Energy-transfer rate as a function of the number of MoS_2 layers. The *dashed line* represents the energy-transfer rate to thick, bulk-like MoS_2, and the *circles* indicate experimental data. Inset: schematic representation of the definition of the thickness (t) and distance (d) parameters. Reprinted with permission from Ref. [54] with a slight modification (copyright 2014, American Chemical Society)

thickness (depicted as numbers in the Figure). Fluorescence lifetime decays of QDs were observed by laser-scanning microscopy (Fig. 14.7b). The fluorescence lifetime of QDs located away from the flake was close to their native lifetime of 20.4 ns, while those of the QDs on top of the MoS_2 were significantly shortened, indicating the strong quenching of the QD excited state by FRET to the MoS_2 nanosheets. Interestingly, the lifetime was dependent on flake thickness, with the strongest QD quenching occurring for the thinnest regions of MoS_2. The differences in QD lifetimes and calculated energy-transfer efficiencies on layered MoS_2 with varying thicknesses can be expressed as 2D mapping images, as shown in Fig. 14.7b and c, respectively. As a result of systematic experiments, the energy-

transfer rates corresponding to the different thicknesses ranging from 1 to 8 layers were determined with the energy-transfer rate in the bulk limit (Fig. 14.7d).

Similarly, organic nanosheets, such as graphitic carbon nitrides [55], hexagonal boron nitrides [56], synthetic 2D polymers [57], and supramolecular metal-complex nanosheets [58], are also promising as novel 2D FRET systems.

FRET is now a promising tool due to its distance dependence; $k_{ET} \propto R^{-6}$ (Eq. 14.2), especially for biological nanoscale analyzes. Moreover, 2D FRET is a promising candidate for accomplishing artificial photosynthesis; an artificial light-harvesting system (which generally requires stepwise efficient FRET processes) and an artificial reaction center complex, a leading candidate in renewable energy production. Hence, nanosheet-based efficient FRET or other photophysical processes are greatly encouraged for future energy and environmental applications.

14.6 Summary

In this chapter, inorganic nanosheet-based photoenergy conversion systems have been briefly reviewed. Some representative works have already reported efficient photoenergy conversion as well as the effective utilization of unique advantages of two-dimensional nanosheets. Novel and more efficient photoenergy conversion systems using inorganic nanosheets with a help of molecules, nanoparticles or other kinds of inorganic nanosheets are highly desired in order to realize future sustainable society.

References

1. Fujishima A, Honda K (1972) Electrochemical photolysis of water at a semiconductor electrode. Nature 238:37–38
2. Osterloh FE (2013) Inorganic nanostructures for photoelectrochemical and photocatalytic water splitting. Chem Soc Rev 42:2294–2320
3. Wang L, Sasaki T (2014) Titanium oxide nanosheets: graphene analogues with versatile functionalities. Chem Rev 114:9455–9486
4. Paek S-M, Jung H, Lee Y-J, Park M, Hwang S-J, Choy J-H (2006) Exfoliation and reassembling route to mesoporous titania nanohybrids. Chem Mater 18:1134–1140
5. Liu G, Wang L, Sun C, Chen Z, Yan X, Cheng L et al (2009) Nitrogen-doped titania nanosheets towards visible light response. Chem Commun 1383–1383
6. Allen MR, Thibert A, Sabio EM, Browning ND, Larsen DS, Osterloh FE (2010) Evolution of physical and photocatalytic properties in the layered titanates $A_2Ti_4O_9$ (A = K, H) and in nanosheets derived by chemical exfoliation. Chem Mater 22:1220–1228
7. Domen K, Kudo A, Shibata M, Tanaka A, Maruya KI, Onishi T (1986) Novel photocatalysts, ion-exchanged $K_4Nb_6O_{17}$, with a layer structure. J Chem Soc Chem Commun 1706–1712
8. Sayama K, Tanaka A, Domen K (1991) Photocatalytic decomposition of water over platinum-intercalated potassium niobate ($K_4Nb_6O_{17}$). J Phys Chem 95:1345–1348

9. Compton OC, Mullet CH, Chiang S, Osterloh FE (2008) A building block approach to photochemical water-splitting catalysts based on layered niobate nanosheets. J Phys Chem C 112:6202–6208
10. Tan B, Wu Y (2006) Dye-sensitized solar cells based on anatase TiO_2 nanoparticle/nanowire composites. J Phys Chem B 110:15932–15938
11. Akatsuka K, Ebina Y, Muramatsu M, Sato T, Hester H, Kumaresan D et al (2007) Photoelectrochemical properties of alternating multilayer films composed of titania nanosheets and Zn porphyrin. Langmuir 23:6730–6736
12. Akatsuka K, Takanashi G, Ebina Y, Haga M-A, Sasaki T (2012) Electronic band structure of exfoliated titanium- and/or niobium-based oxide nanosheets probed by electrochemical and photoelectrochemical measurements. J Phys Chem C 116:12426–12433
13. Irie M, Kobatake S, Horichi M (2001) Reversible surface morphology changes of a photochromic diarylethene single crystal by photoirradiation. Science 291:1769–1772
14. Yu Y, Nakano M, Ikeda T (2003) Directed bending of a polymer film by light. Nature 425:145–145
15. Nabetani Y, Takamura H, Hayasaka Y, Shimada T, Takagi S, Tachibana H et al (2011) A photoactivated artificial muscle model unit: reversible, photoinduced sliding of nanosheets. J Am Chem Soc 133:17130–17133
16. Nabetani Y, Takamura H, Hayasaka Y, Sasamoto S, Tanamura Y, Shimada T et al (2013) An artificial muscle model unit based on inorganic nanosheet sliding by photochemical reaction. Nanoscale 5:3182
17. Perrin JB (1924) Fluorescence et lois générales relatives aux vitesses de réaction. Comptes rendus hebdomadaires des séances de l'Académie des Sci 178:1401–1406
18. Förster Th (1946) Energiewanderung und Fluoreszenz. Naturwissenschaften 6:166–175
19. Förster Th (1948) Zwischenmolekulare Energiewanderung und Fluoreszenz. Ann Phys 1–2:55–75
20. Baumann J, Fayer MD (1986) Excitation transfer in disordered two-dimensional and anisotropic three-dimensional systems: effects of spatial geometry on time-resolved observables. J Chem Phys 85:4087
21. Kelley RF, Lee SJ, Wilson TM, Nakamura Y, Tiede DM, Osuka A et al (2008) Intramolecular energy transfer within butadiyne-linked chlorophyll and porphyrin dimer-faced, self-assembled prisms. J Am Chem Soc 130:4277–4284
22. Hoffman JB, Choi H, Kamat PV (2014) Size-dependent energy transfer pathways in cdse quantum dot-squaraine light-harvesting assemblies: förster versus dexter. J Phys Chem C 118:18453–18461
23. Zhang X, Marocico CA, Lunz M, Gerard VA, Gun'ko YK, Lesnyak V et al (2014) Experimental and theoretical investigation of the distance dependence of localized surface plasmon coupled förster resonance energy transfer. ACS Nano 8:1273–1283
24. Becker K, Lupton JM, Müller J, Rogach AL, Talapin DV, Weller H et al (2006) Electrical control of Förster energy transfer. Nat Mater 5:777–781
25. Inagaki S, Ohtani O, Goto Y, Okamoto K, Ikai M, Yamanaka K-I et al (2009) Light harvesting by a periodic mesoporous organosilica chromophore. Angew Chem Int Ed 48:4042–4046
26. Hildebrandt N, Wegner KD, Algar WR (2014) Luminescent terbium complexes: superior Förster resonance energy transfer donors for flexible and sensitive multiplexed biosensing. Coord Chem Rev 273–274:125–138
27. Frischmann PD, Mahata K, Würthner F (2013) Powering the future of molecular artificial photosynthesis with light-harvesting metallosupramolecular dye assemblies. Chem Soc Rev 42:1847–1870
28. Silvi S, Credi A (2015) Luminescent sensors based on quantum dot-molecule conjugates. Chem Soc Rev 44:4275–4289
29. McDermott G, Prince SM, Freer AA, Hawthornthwaite-Lawless AM, Papiz MZ, Cogdell RJ et al (1995) Crystal structure of an integral membrane light-harvesting complex from photosynthetic bacteria. Nature 374:517–521

30. Takagi S, Tryk DA, Inoue H (2002) Photochemical energy transfer of cationic porphyrin complexes on clay surface. J Phys Chem B 106:5455–5460
31. Ishida Y, Shimada T, Takagi S (2014) Surface-fixation induced emission of porphyrazine dye by a complexation with inorganic nanosheets. J Phys Chem C 118:20466–20471
32. Villemure G, Detellier C, Szabo AG (1986) Fluorescence of clay-intercalated methylviologen. J Am Chem Soc 108:4658–4659
33. Shichi T, Takagi K (2000) Clay minerals as photochemical reaction fields. J Photochem Photobiol C Photochem Rev 1:113–130
34. Bujdák J (2006) Effect of the layer charge of clay minerals on optical properties of organic dyes. A review. Appl Clay Sci 34:58–73
35. Ghosh PK, Bard AJ (1984) Photochemistry of tris (2, 2′-bipyridyl) ruthenium (II) in colloidal clay suspensions. J Phys Chem 88:5519–5526
36. Takagi S, Shimada T, Eguchi M, Yui T, Yoshida H, Tryk DA et al (2002) High-density adsorption of cationic porphyrins on clay layer surfaces without aggregation: the size-matching effect. Langmuir 18:2265–2272
37. Takagi S, Shimada T, Ishida Y, Fujimura T, Masui D, Tachibana H et al (2013) Size-matching effect on inorganic nanosheets: control of distance, alignment, and orientation of molecular adsorption as a bottom-up methodology for nanomaterials. Langmuir 29:2108–2119
38. Ishida Y, Shimada T, Masui D, Tachibana H, Inoue H, Takagi S (2011) Efficient excited energy transfer reaction in clay/porphyrin complex toward an artificial light-harvesting system. J Am Chem Soc 133:14280–14286
39. Ishida Y, Kulasekharan R, Shimada T, Ramamurthy V, Takagi S (2014) Supramolecular-surface photochemistry: supramolecular assembly organized on a clay surface facilitates energy transfer between an encapsulated donor and a free acceptor. J Phys Chem C 118:10198–10203
40. Ishida Y, Kulasekharan R, Shimada T, Takagi S, Ramamurthy V (2013) Efficient singlet-singlet energy transfer in a novel host-guest assembly composed of an organic cavitand, aromatic molecules, and a clay nanosheet. Langmuir 29:1748–1753
41. Kulasekharan R, Ramamurthy V (2011) New water-soluble organic capsules are effective in controlling excited-state processes of guest molecules. Org Lett 13:5092–5095
42. Ishida Y, Shimada T, Takagi S (2013) Artificial light-harvesting model in a self-assembly composed of cationic dyes and inorganic nanosheet. J Phys Chem C 117:9154–9163
43. Ishida Y, Shimada T, Tachibana H, Inoue H, Takagi S (2012) Regulation of the collisional self-quenching of fluorescence in clay/porphyrin complex by strong host-guest interaction. J Phys Chem A 116:12065–12072
44. Ishida Y, Fujimura T, Masui D, Shimada T, Tachibana H, Inoue H et al (2011) What lowers the efficiency of an energy transfer reaction between porphyrin dyes on clay surface? Clay Sci 15:169–174
45. Rao CNR, Sood AK, Subrahmanyam KS, Govindaraj A (2009) Graphene: the new two-dimensional nanomaterial. Angew Chem Int Ed 48:7752–7777
46. Morales-Narváez E, Merkoçi A (2012) Graphene oxide as an optical biosensing platform. Adv Mater 24:3298–3308
47. Piao Y, Liu F, Seo TS (2011) The photoluminescent graphene oxide serves as an acceptor rather than a donor in the fluorescence resonance energy transfer pair of Cy3.5-graphene oxide. Chem Commun 47:12149–12151
48. Liu F, Choi JY, Seo TS (2010) Graphene oxide arrays for detecting specific DNA hybridization by fluorescence resonance energy transfer. Biosens Bioelectron 25:2361–2365
49. Balapanuru J, Yang J-X, Xiao S, Bao Q, Jahan M, Polavarapu L et al (2010) A graphene oxide-organic dye ionic complex with DNA-sensing and optical-limiting properties. Angew Chem Int Ed 49:6549–6553
50. Dong H, Gao W, Yan F, Ji H, Ju H (2010) Fluorescence resonance energy transfer between quantum dots and graphene oxide for sensing biomolecules. Anal Chem 82:5511–5517

51. Zhu C, Zeng Z, Li H, Li F, Fan C, Zhang H (2013) Single-layer MoS_2-based nanoprobes for homogeneous detection of biomolecules. J Am Chem Soc 135:5998–6001
52. Ha HD, Han DJ, Choi JS, Park M, Seo TS (2014) Dual role of blue luminescent MoS_2 quantum dots in fluorescence resonance energy transfer phenomenon. Small 10:3858–3862
53. Scheuschner N, Ochedowski O, Kaulitz A-M, Gillen R, Schleberger M, Maultzsch J (2014) Photoluminescence of freestanding single- and few-layer MoS_2. Phys Rev B 89:125406
54. Prins F, Goodman AJ, Tisdale WA (2014) Reduced dielectric screening and enhanced energy transfer in single- and few-layer MoS_2. Nano Lett 14:6087–6091
55. Wang Q, Wang W, Lei J, Xu N, Gao F, Ju H (2013) Fluorescence quenching of carbon nitride nanosheet through its interaction with DNA for versatile fluorescence sensing. Anal Chem 85:12182–12188
56. Song L, Ci L, Lu H, Sorokin PB, Jin C, Ni J et al (2010) Large scale growth and characterization of atomic hexagonal boron nitride layers. Nano Lett 10:3209–3215
57. Sakamoto J, van Heijst J, Lukin O, Schlüter AD (2009) Two-dimensional polymers: just a dream of synthetic chemists? Angew Chem Int Ed 48:1030–1069
58. Sakamoto R, Takada K, Sun X, Pal T, Tsukamoto T, Phua EJH et al (2016) The coordination nanosheet (CONASH). Coordin Chem Rev 320–321:118–128